A selective class of inhibitors for the CLC-Ka chloride ion channel

Anna K. Koster[a,b,1], Chase A. P. Wood[b,1], Rhiannon Thomas-Tran[a], Tanmay S. Chavan[b], Jonas Almqvist[c], Kee-Hyun Choi[d], J. Du Bois[a,2], and Merritt Maduke[b,2]

[a]Department of Chemistry, Stanford University, Stanford, CA 94305; [b]Department of Molecular and Cellular Physiology, Stanford University School of Medicine, Stanford, CA 94305; [c]Department of Cell and Molecular Biology, Uppsala University, 751 24 Uppsala, Sweden; and [d]Materials and Life Science Research Division, Korea Institute of Science and Technology, 02792 Seoul, Republic of Korea

Edited by Richard W. Aldrich, The University of Texas at Austin, Austin, TX, and approved March 21, 2018 (received for review December 7, 2017)

CLC proteins are a ubiquitously expressed family of chloride-selective ion channels and transporters. A dearth of pharmacological tools for modulating CLC gating and ion conduction limits investigations aimed at understanding CLC structure/function and physiology. Herein, we describe the design, synthesis, and evaluation of a collection of *N*-arylated benzimidazole derivatives (BIMs), one of which (BIM1) shows unparalleled (>20-fold) selectivity for CLC-Ka over CLC-Kb, the two most closely related human CLC homologs. Computational docking to a CLC-Ka homology model has identified a BIM1 binding site on the extracellular face of the protein near the chloride permeation pathway in a region previously identified as a binding site for other less selective inhibitors. Results from site-directed mutagenesis experiments are consistent with predictions of this docking model. The residue at position 68 is 1 of only ∼20 extracellular residues that differ between CLC-Ka and CLC-Kb. Mutation of this residue in CLC-Ka and CLC-Kb (N68D and D68N, respectively) reverses the preference of BIM1 for CLC-Ka over CLC-Kb, thus showing the critical role of residue 68 in establishing BIM1 selectivity. Molecular docking studies together with results from structure–activity relationship studies with 19 BIM derivatives give insight into the increased selectivity of BIM1 compared with other inhibitors and identify strategies for further developing this class of compounds.

chloride channel | molecular probes | electrophysiology

CLC proteins are a class of highly selective chloride (Cl^-) ion channels and transporters that are essential for proper physiological function, including electrical signaling in muscles and neurons and regulation of ion homeostasis (1–4). CLCs possess a unique homodimeric, double-barreled structure and operate through distinct gating (opening/closing) mechanisms (5–10), which differ markedly from those of sodium, potassium, and calcium channels. While researchers in the field have made important progress toward understanding general CLC structural dynamics and physiology, achieving a precise mechanistic understanding of these processes has remained a challenge (11–13). Small molecules that bind and modulate specific CLC homologs could serve as valuable tools for untangling the complex gating behaviors and diverse physiological functions within the CLC family. Small molecule modulators of CLCs also hold promise as therapeutic leads (14, 15). For certain kidney-related disorders, two CLC homologs, CLC-Ka and CLC-Kb, are particularly compelling targets due to their important roles in maintaining electrolyte balance. In humans, CLC-Kb loss-of-function mutations result in type III Bartter's syndrome, a salt-wasting disorder characterized by low blood pressure (16). This phenotype suggests CLC-Kb as a potential target for antihypertensive therapeutics. Similarly, mouse KO models show that CLC-Ka Cl^- transport is necessary for concentration of urine (17, 18) and thus suggest that inhibitors could be used to treat hyponatremia (19), a condition in which blood concentrations of sodium are low. Hyponatremia develops when the kidneys fail to excrete water efficiently and can occur in patients with heart failure, cirrhosis, renal failure, or other conditions (19, 20). Treatment of hyponatremia can be challenging, and without intervention, permanent neurological damage can occur (20, 21). Selectivity between small molecule inhibitors of CLC-Ka and CLC-Kb is critical for any clinical application, as these two channels are also expressed in the inner ear, where they play critical but redundant roles: disruption of both homologs results in deafness, while disruption of either individually has no effect on hearing (22).

The development of selective small molecules that specifically target either CLC-Ka or CLC-Kb poses a formidable challenge in ligand design due to the >90% sequence identity between the two homologs. Prior reports of CLC inhibitors largely describe low-affinity (midmicromolar to millimolar IC_{50}) compounds that lack selectivity. The most potent CLC inhibitor known is a peptide toxin, GaTx2, which selectively inhibits CLC-2 with an IC_{50} of ∼20 pM. However, despite its potency, GaTx2 inhibition saturates at ∼50% (23), thus limiting its use as a pharmacological probe. Accordingly, we have been motivated to identify small molecule inhibitors of specific CLCs. Two classes of small molecule inhibitors have been reported to display moderate potency and selectivity for CLC-Ka over CLC-Kb. The first, a collection of stilbene disulfonates, is a promiscuous class of anion transport inhibitors (24–26). One of these, 4,4′-diisothiocyano-2,2′-stilbenedisulfonic acid (DIDS), was used as a chemical tool to corroborate the dimeric architecture of the Torpedo CLC-0 channel (27). Subsequently, our laboratories showed that DIDS hydrolyzes in buffer solution to form polythiourea oligomers, which are more

Significance

Chloride ion channels and transporters (CLCs) are critical to cardiovascular, neurological, and musculoskeletal function. Small molecules capable of selectively inhibiting CLCs would serve as valuable tools for investigating CLC function and would have potential applications for treating CLC-related disorders. The lack of such agents has impeded efforts to study this family of proteins. This work introduces a class of inhibitors with unprecedented selectivity for a single CLC homolog, CLC-Ka. Insights gained through experiments to validate a predicted ligand binding site and to evaluate structure–activity relationships rationalize inhibitor potency and CLC-Ka selectivity. Our findings provide tools for studies of CLC-Ka function and will assist subsequent efforts to advance specific molecular probes for different CLC homologs.

Author contributions: A.K.K., C.A.P.W., J.A., K.-H.C., J.D.B., and M.M. designed research; A.K.K., C.A.P.W., R.T.-T., T.S.C., J.A., and K.-H.C. performed research; A.K.K., C.A.P.W., R.T.-T., T.S.C., J.A., K.-H.C., J.D.B., and M.M. analyzed data; and A.K.K., J.D.B., and M.M. wrote the paper with contributions from all authors.

The authors declare no conflict of interest.

This article is a PNAS Direct Submission.

[1]A.K.K. and C.A.P.W. contributed equally to this work.

[2]To whom correspondence may be addressed. Email: jdubois@stanford.edu or maduke@stanford.edu.

This article contains supporting information online at www.pnas.org/lookup/suppl/doi:10.1073/pnas.1720584115/-/DCSupplemental.

potent antagonists of CLC-0, CLC-Ka, and CLC-ec1 than DIDS itself (28). A DIDS pentamer (Fig. 1*A*) is the most potent and selective nonpeptidic CLC inhibitor known, with an IC_{50} against CLC-Ka of 0.5 μM and ∼100-fold increased IC_{50} against CLC-Kb (28). However, structure–activity relationship (SAR) studies and further development of DIDS-based inhibitors are severely hampered due to the low water solubility of these oligomeric molecules as well as the synthetic challenges of systematically modifying the DIDS scaffold. A second class of CLC inhibitors is based on an aryl-substituted benzofuran carboxylic acid (29, 30). The most notable of these compounds, MT-189 and SRA-36 (Fig. 1*B*), are ∼10-fold less potent than the DIDS pentamer but more amenable to synthetic manipulation. While SRA-36 inhibits both CLC-Ka and CLC-Kb with equal potency, MT-189 has a nearly threefold greater apparent affinity for CLC-Ka over CLC-Kb (IC_{50} = 7 vs. 20 μM) (29).

Results and Discussion

Inhibitor Design and Synthesis. Our design of *N*-arylated benzimidazole derivatives (BIMs) follows from previous reports by Liantonio et al. (29, 30) that describe the inhibitory effects of benzofuran carboxylate compounds against CLC-Ka and CLC-Kb (29, 30). In these studies, the most potent CLC-K biaryl inhibitors were found to be conformationally restricted molecules that favor a twisted, noncoplanar structure of the two aromatic rings (Fig. 1*B*) (29). We hypothesized that an *N*-arylated benzimidazole would possess an analogous molecular topology. This substituted heterocycle could be easily assembled from commercially available building blocks (Scheme 1), facilitating access to a collection of structurally disparate derivatives. Replacing the carboxylate group of MT-189 with a sulfonate anion was also considered an important design element to increase selectivity for CLC-Ka over CLC-Kb, a decision based on our earlier finding that the sulfonated CLC inhibitor DIDS exhibits greater homolog selectivity than MT-189 (28). The resulting heterocyclic structure, BIM1, is shown in Fig. 1*C*.

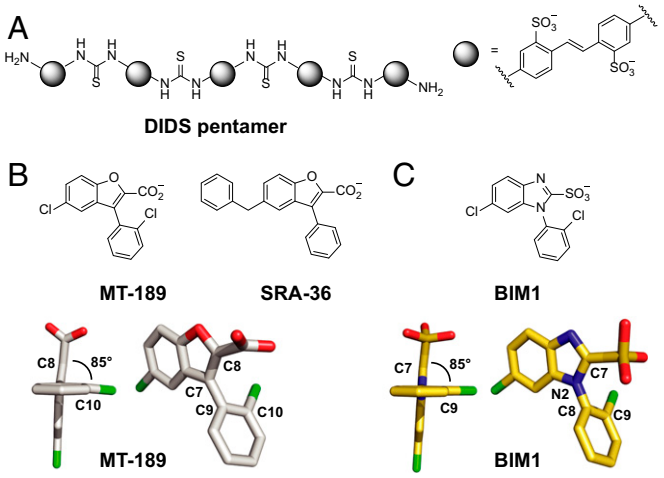

Fig. 1. Design of the BIM scaffold using known CLC-K inhibitors as inspiration. (*A*) The DIDS pentamer inhibits CLC-Ka with an IC_{50} of 0.5 μM and exhibits ∼100-fold reduced potency toward CLC-Kb. (*B*) The benzofuran carboxylates, which are synthetically more tractable than the DIDS oligomers, inhibit CLC-Ka and CLC-Kb with apparent affinities in the low micromolar range. MT-189 shows approximately threefold selectivity for CLC-Ka over CLC-Kb. *Lower* illustrates the noncoplanar conformation of MT-189, which is predicted to be an essential structural feature for inhibition (29). (*C*) The design of BIM1, a benzimidazole sulfonate, is inspired by the benzofuran lead compounds shown in *B* and by the sulfonated DIDS inhibitors (*A*). *Lower* shows a hypothesized noncoplanar conformation for BIM1.

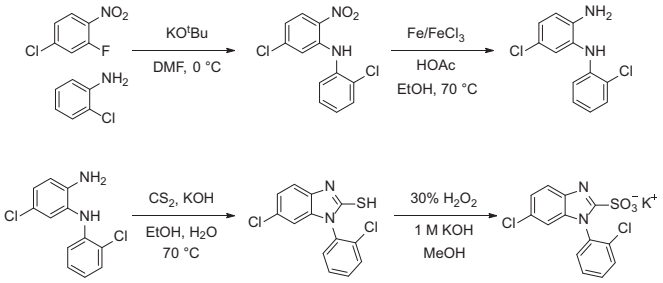

Scheme 1. Synthesis of BIMs.

BIM1 Exhibits Enhanced Homolog Selectivity. CLC-K channels were expressed in *Xenopus* oocytes, and two-electrode voltage clamp (TEVC) recording was used to measure currents before and after perfusion of inhibitor solutions. At 100 μM, BIM1 is an effective inhibitor of CLC-Ka but shows markedly reduced activity toward CLC-Kb (Fig. 2 *A* and *B* and Table S1). The IC_{50} for BIM1 against CLC-Ka, 8.5 ± 0.4 μM, is similar to that reported for MT-189 (7.0 ± 1.0 μM) (29). In contrast, the potency of BIM1 against CLC-Kb is significantly diminished [IC_{50} = 200 ± 20 μM for BIM1 (Fig. 2*C*) vs. 20 ± 2 μM for MT-189 (29)]. The identification of BIM1, which displays >20-fold selectivity for CLC-Ka over CLC-Kb, is notable given that these two channels are ∼90% identical in amino acid sequence. The next closest homologs within the CLC family, CLC-1 and CLC-2 (40–45% identical to the CLC-K channels), are insensitive to BIM1 at 100 μM (Fig. 3). These data strongly suggest that BIM1 will selectively inhibit CLC-Ka over other ion channels and transporters found in the plasma membrane, a notable advance given the promiscuity of many Cl^- channel inhibitors (31).

Computational Modeling to Predict the BIM Binding Site. To gain insight into the location of the BIM1 binding site, we generated a homology model of human CLC-Ka based on the crystal structures of the eukaryotic CLC transporter *Cyanidioschyzon merolae* (cm)CLC [Protein Data Bank (PDB) ID code 3org] (32) and the water-soluble domain of human CLC-Ka [PDB ID code 2pfi (33)]. Computational docking of BIM1 to the extracellular surface of our CLC-Ka homology model identified a binding site near residue 68 (Fig. 4), a site known to affect channel sensitivity to MT-189 (29, 34) as well as a variety of other known CLC-Ka inhibitors (3-phenyl-*p*-chlorophenoxy-propionic acid, DIDS, and flufenamic acid derivatives) (34–36). In most CLC homologs, including CLC-Kb, this residue is an aspartate. CLC-Ka is unique among the human homologs in that it contains a neutral asparagine at this position, 1 of only ∼20 residues on the extracellular face of CLC-Ka that differ from CLC-Kb. A second ligand–channel interaction identified by our model is an electrostatic interaction of the BIM1 sulfonate group with K165, a residue located in the extracellular vestibule of the channel (Fig. 4).

Testing Predictions of the Computational Docking. In our CLC model, the proximity of N68 to the sulfonate group of BIM1 (Fig. 4) predicts that introduction of an acidic residue at this position will weaken the CLC-Ka–BIM1 interaction. CLC-Ka N68D was expressed in *Xenopus* oocytes, and the sensitivity of the mutant channel to BIM1 was evaluated. Consistent with our model, the N68D mutation decreased sensitivity to BIM1 from an IC_{50} of 8.5 ± 0.4 to 114 ± 14 μM (Fig. 5 and Table S2). This loss in potency parallels that observed for MT-189 against this same mutant (IC_{50} of 7.0 ± 1.0 vs. 54 ± 8 μM) (29). As another test of the model, the complementary mutation, D68N, was introduced into CLC-Kb. This mutation increased sensitivity to BIM1 from an IC_{50} of 200 ± 20 to 55 ± 36 μM (Fig. 5 and Table S2). Thus, the preference of BIM1 for CLC-Ka over CLC-Kb is eliminated with this single-point mutation. This experiment shows that the amino acid at position 68 is critical for establishing BIM1 selectivity

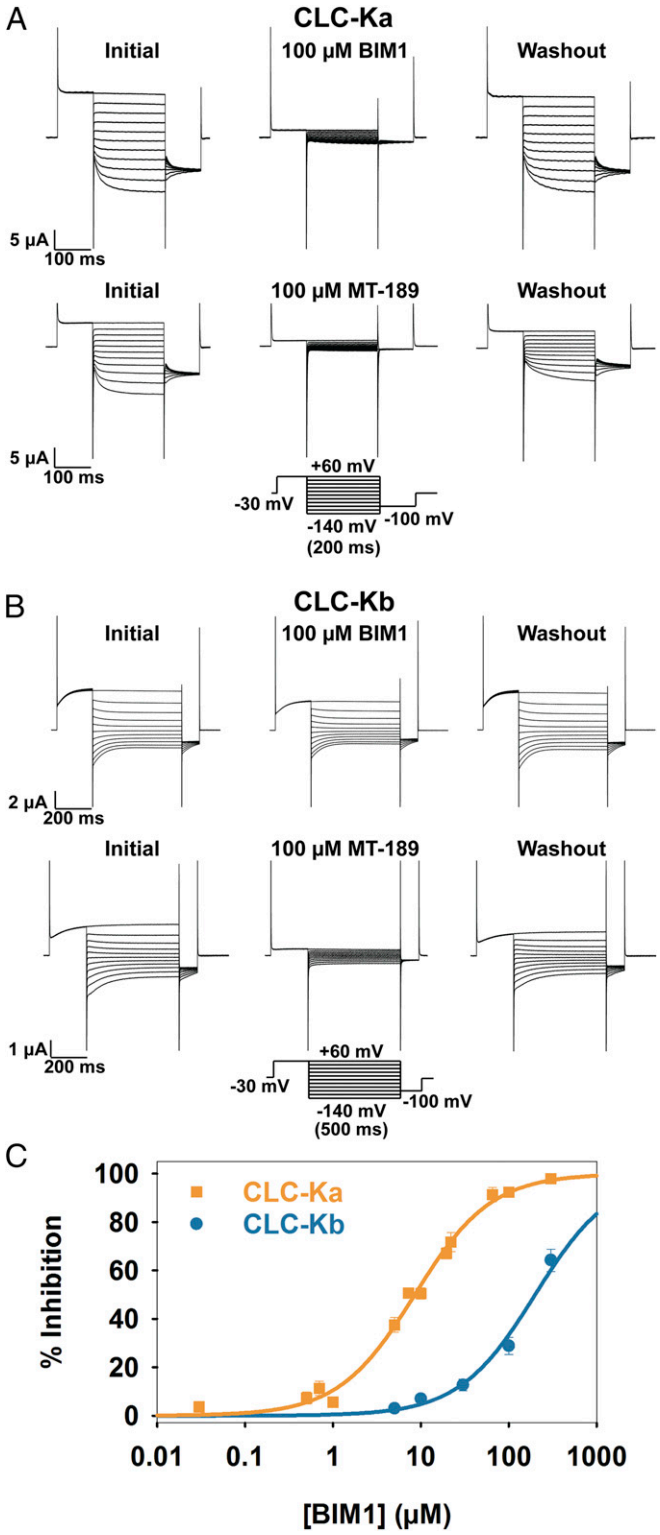

Fig. 2. BIM1 is selective for CLC-Ka over CLC-Kb. (*A*) Representative CLC-Ka currents, recorded using TEVC, before application, after application, and after washout of 100 μM BIM1 (*Upper*) or MT-189 (*Lower*). (*B*) Representative CLC-Kb currents showing sensitivity to 100 μM BIM1 and MT-189 (as in *A*). (*C*) Summary data for BIM1 inhibition at +60 mV. [Inhibition is not significantly voltage-dependent (Fig. S1).] Each data point represents the mean ± SEM for measurements on 3–15 oocytes at each concentration (Table S1). Oocytes were obtained from multiple (>10) batches of oocytes injected and measured on separate occasions. For CLC-Ka, the solid line is a fit of the data to the equation: $I = (I_{max} \times [BIM1]^n)/(IC_{50}{}^n + [BIM1]^n)$, where I is the percentage inhibition, I_{max} is the maximal inhibition, IC_{50} is 8.5 ± 0.4 μM, and n is the Hill coefficient (0.99). For CLC-Kb, the solid line is a fit to the same equation but with I_{max} and n fixed at 100 and 1.0, respectively, yielding a value of 200 ± 20 μM for the IC_{50} of BIM1 against CLC-Kb.

between CLC-Ka and CLC-Kb and is consistent with a predicted direct interaction between BIM1 and this residue.

A second BIM1–protein interaction apparent in our CLC-Ka homology model—that between the sulfonate group of the inhibitor and K165—was more challenging to validate through mutagenesis experiments. It has been shown that mutation of K165 to a neutral residue (A, C, H, or Q) prevents functional expression (37). Thus, as an alternative approach to examining the sulfonate–K165 interaction, we first varied the extracellular pH of our recording solution to alter the protonation state of the lysine residue. Changes in the BIM1 IC_{50} as a function of pH would be expected if an attractive electrostatic interaction between K165 and the anionic BIM1 sulfonate group is present. Consistent with this prediction, raising the pH from 7.6 to 9.5 decreases inhibition of CLC-Ka by BIM1 (from 75 ± 3 to 24 ± 4% at 22 μM BIM1) (Fig. 6 *A* and *C*). To test that the reduction in BIM1 potency is due to the neutralization of K165 (as opposed to another titratable residue on CLC-Ka), we examined the effect of an Arg mutation at K165. According to previous work, K165R is the only mutation tolerated at this position (37). At pH 9.5, the protonated form of Arg (K165R) should be present to a greater extent than the protonated form of Lys (K165) due to the inherent difference in pK_a between these two residues. The pK_a values for Lys and Arg in alanine pentapeptides are 10.4 and 12.3, respectively (38). In the folded protein environment, these pK_a values will shift (38); however, the relative difference in pK_a should persist. As such, inhibition of K165R by BIM1 should be less sensitive to pH than WT CLC-Ka. At pH 7.6, BIM1 inhibits the CLC-Ka K165R channel with similar potency to the WT (75 ± 3 vs. 72 ± 5% inhibition at 22 μM BIM1) (Fig. 6). In contrast, at pH 9.5, K165R is more sensitive to BIM1 than the WT channel is (inhibition of 54 ± 7 vs. 26 ± 3% at 22 μM BIM1) (Fig. 6). Together, these results support the hypothesis that the positively charged K165 residue is positioned in or near the inhibitor binding site.

Comparison with an Alternative Docking Model. In 2016, Liantonio et al. (30) disclosed results from a computational study, in which MT-189 and related inhibitors were docked to CLC-Ka. Our model of CLC-Ka docked to BIM1 shares many similarities, including specific interactions with N68 and K165 (Fig. 4). However, the model by Liantonio et al. also identifies ligand contacts with I263 and H346. In our model, these loop residues are far removed from the inhibitor binding site (Fig. 7*A*). The difference between the two docking results likely arises from differences in the structural templates used to generate the CLC-Ka homology models, which vary significantly in their loop regions (discussion is in *SI Discussion of CLC-K Homology Models*).

To distinguish between the two computational models, we evaluated the contribution of H346 to BIM1 binding through site-directed mutagenesis experiments. Application of 15 μM BIM1 to H346A inhibited current by 65 ± 3%, which is indistinguishable from the inhibition observed with WT CLC-Ka: 62 ± 5% (Fig. 7 and Fig. S2). In addition, the H346A mutation did not affect the sensitivity of channel binding to the benzofuran derivative MT-189 (depicted in Fig. 1*B*). These results (Fig. 7 and Fig. S2) favor a model in which this residue is not involved in either benzofuran or benzimidazole binding.

Comparison with Homology Models Based on Bovine CLC-K Structures. After our initial mutagenesis studies to identify the BIM binding site, two high-resolution structures of the bovine chloride channel bCLC-K were disclosed (39) [The two structures, although distinct, are highly similar to one another (details are in *Materials and Methods*).] Because of the significantly greater amino acid sequence similarity of bCLC-K with CLC-Ka and CLC-Kb

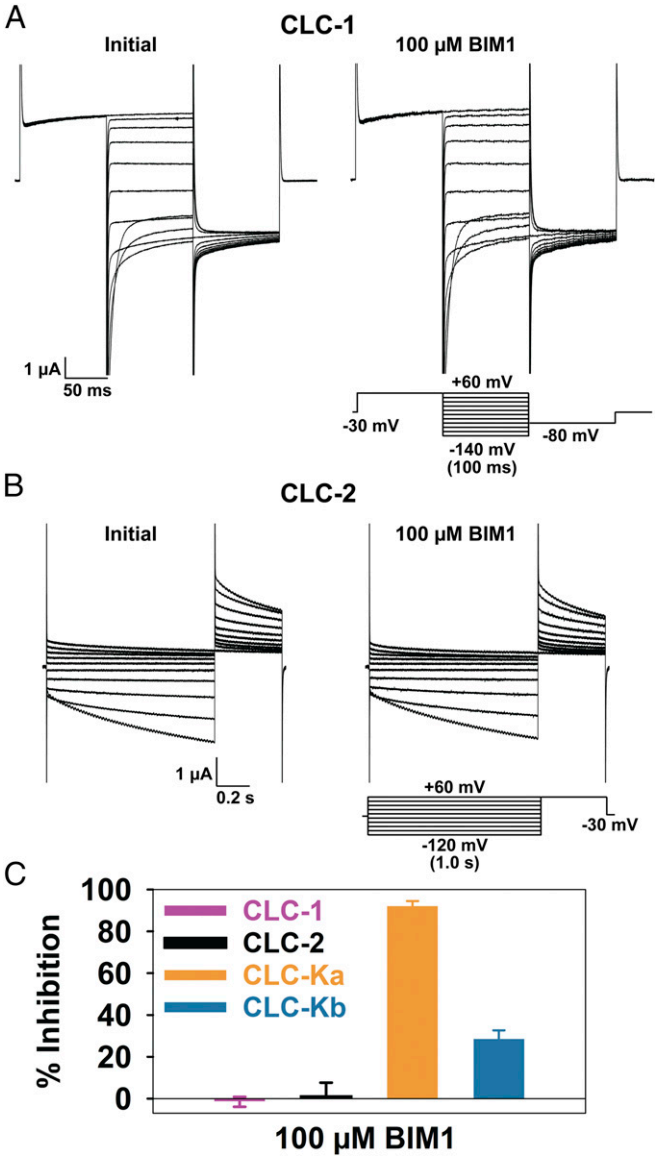

Fig. 3. Selectivity of BIM1 among mammalian CLC homologs. Representative currents from *Xenopus* oocytes expressing CLC-1 (*A*) or CLC-2 (*B*) shown before and after application of 100 μM BIM1. (*C*) Summary inhibition data (± SEM) for 100 μM BIM1 on CLC-1 (n = 8), CLC-2 (n = 8), CLC-Ka (n = 9), and CLC-Kb (n = 6). Inhibition is reported for data at +60 mV (CLC-Ka, CLC-Kb, and CLC-1) or −120 mV (CLC-2). For CLC-1 and CLC-2, inhibition is not significantly different from zero (P = 0.55 and P = 0.84, respectively).

(84% sequence identity) compared with the cmCLC transporter on which our original model was based (32% identity), we developed updated CLC-Ka homology models derived from the bCLC-K structures. Consistent with our original model, docking of BIM1 to either of these constructs favors an extracellular binding pocket composed of residues N68 and K165, with H346 and I263 distant from the inhibitor binding site. Although both original and updated CLC-Ka homology models locate N68 and K165 in the binding pocket, the collection and orientation of amino acids within this region vary significantly between models. A summary of these findings is presented in Fig. S3.

SAR Studies. To evaluate the effects of molecular structure on inhibitor potency and selectivity, we synthesized a panel of 19 BIM inhibitors substituted at positions $\mathbf{R^1}$–$\mathbf{R^6}$ (Fig. 8). Using TEVC, CLC-Ka and CLC-Kb currents were measured before and after application of each compound at 100 μM (as in Fig. 2). Compounds inhibiting >80% of the CLC-Ka current at 100 μM (Fig. 8 and Table S3) were also screened at 5 μM for a more accurate comparison of potency (Fig. S4 and Table S4). BIM15 and BIM16 were found to be slightly more potent than BIM1, inhibiting CLC-Ka by 54 and 72%, respectively, at 5 μM compared with 37% for BIM1; however, this was accompanied by a loss in selectivity (discussed below).

Effects on inhibitor potency. To assess the influence of each BIM substituent, the potency against CLC-Ka of every inhibitor was compared with an equivalent compound bearing a hydrogen atom at each of the positions $\mathbf{R^1}$–$\mathbf{R^6}$. To begin, $\mathbf{R^1}$ was substituted with a carboxylate, a sulfonate, or a hydrogen atom. Consistent with an electrostatic interaction in the inhibitor binding site (Fig. 4), a negatively charged group at $\mathbf{R^1}$ is necessary for inhibitor efficacy (comparing inhibition with 100 μM compound) (Fig. 8). Replacement of $-SO_3^-$ or $-CO_2^-$ with a hydrogen atom (BIM3 and BIM6) renders these compounds inactive against CLC-Ka.

At position $\mathbf{R^2}$, the presence of either -Cl or -Br (BIM1 and BIM11) moderately increases the percentage of inhibition relative to BIM10 ($\mathbf{R^2}$ = H) (Fig. 8 and Table S3). A similar effect is noted for substitution at position $\mathbf{R^6}$ with -Cl or -Br in place of -H (BIM1 and BIM7 vs. BIM8) (Fig. 8 and Table S3). If -Cl is included at both $\mathbf{R^2}$ and $\mathbf{R^6}$ (BIM1), the effect on potency is additive compared with monohalogenated compounds (BIM8 and BIM10). The identity of the halogen atom at positions $\mathbf{R^2}$ and $\mathbf{R^6}$ is inconsequential, with both -Cl and -Br compounds showing the same efficacy at 5 μM (Fig. S4 and Table S4). In comparison with $\mathbf{R^2}$ and $\mathbf{R^6}$, substituting -Cl or -Br at $\mathbf{R^5}$ (BIM12 and BIM13) does not improve BIM efficacy. These compounds are weakly potent and have similar affinity to BIM8 ($\mathbf{R^6}$ = H) (Fig. 8 and Table S3).

To probe the steric environment of the binding pocket surrounding the benzimidazole and *N*-phenyl rings, each of the positions $\mathbf{R^3}$–$\mathbf{R^6}$ was substituted with a -Ph group. For compounds substituted at position $\mathbf{R^5}$ (BIM 14), there is no effect on potency relative to BIM1, while for position $\mathbf{R^6}$ (BIM4, BIM5), there is a negative effect (Fig. 8 and Table S3). Substitution at $\mathbf{R^3}$ or $\mathbf{R^4}$ (BIM15 and BIM16) produces the opposite result to $\mathbf{R^6}$, an enhancement in potency relative to BIM1 (Fig. 8 and Table S3). By contrast, the introduction of a secondary amide group at an equivalent position, $\mathbf{R^3}$ (BIM19), results in a reduction in potency (Fig. 8). Collectively, these findings suggest that the *N*-aryl group of the BIM ligands occupies a rather large void space in the receptor site that can accommodate $\mathbf{R^3}$ and $\mathbf{R^4}$ substituents, with hydrophobic phenyl groups favored over the more polar amide substituent.

Effects on inhibitor selectivity. To evaluate the effect of each substituent on inhibitor selectivity, we compared the ratio of CLC-Kb/CLC-Ka percent inhibition at 100 μM for all 19 BIMs (Fig. 8 and Fig. S5). Substitution at $\mathbf{R^1}$ with $-CO_2^-$ (BIM2) instead of

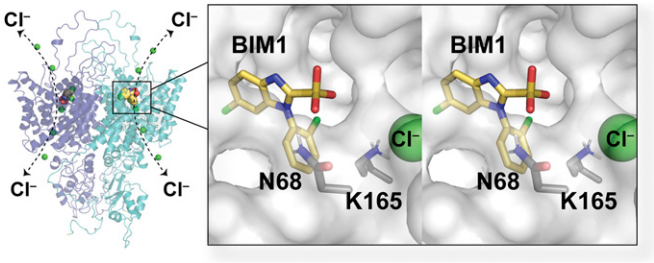

Fig. 4. BIM1 docking to a CLC-Ka homology model. The CLC-Ka homology model viewed from the side. Subunits of the homodimer are colored purple and cyan, and BIM1 is docked to each subunit near the extracellular side of the Cl^- permeation pathway. *Right* shows a close-up stereoview of the BIM binding site. Residues predicted to interact with BIM1 and tested in mutagenesis experiments (N68 and K165) are shown in stick representation. This initial model was constructed using cmCLC (PDB ID code 3org) as a template.

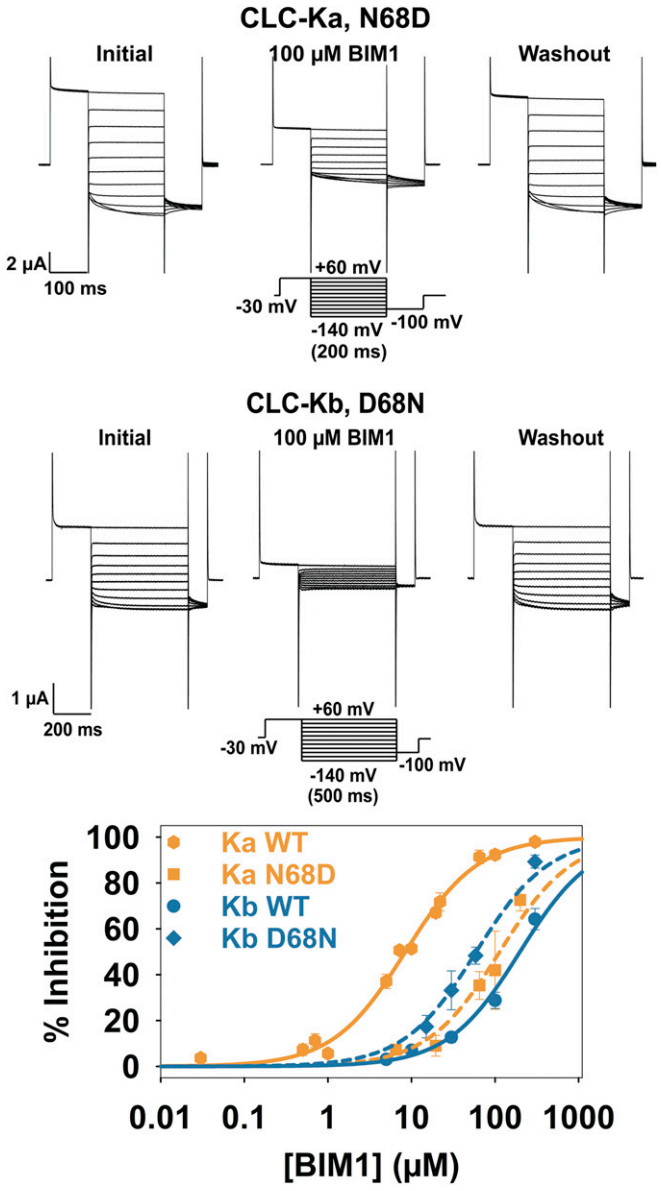

Fig. 5. Testing the docking model: effect of residue 68 mutations. Representative currents for CLC-Ka and CLC-Kb N68/D68 mutants and the respective response to BIM1. The summary graph shows the mean for measurements on two to four oocytes at each concentration. Error bars show either the range of the data points (for $n = 2$) or the SEM (for $n = 3$–4) (Table S2). Oocytes were from two (CLC-Kb D68N) or three (CLC-Ka N68D) batches injected and measured on separate occasions. For comparison, results for WT channels are reproduced from Fig. 2. Dashed curves are fit as described in Fig. 2, with IC_{50} values of 114 ± 14 μM (CLC-Ka N68D) and 60 ± 5 μM (CLC-Kb D68N).

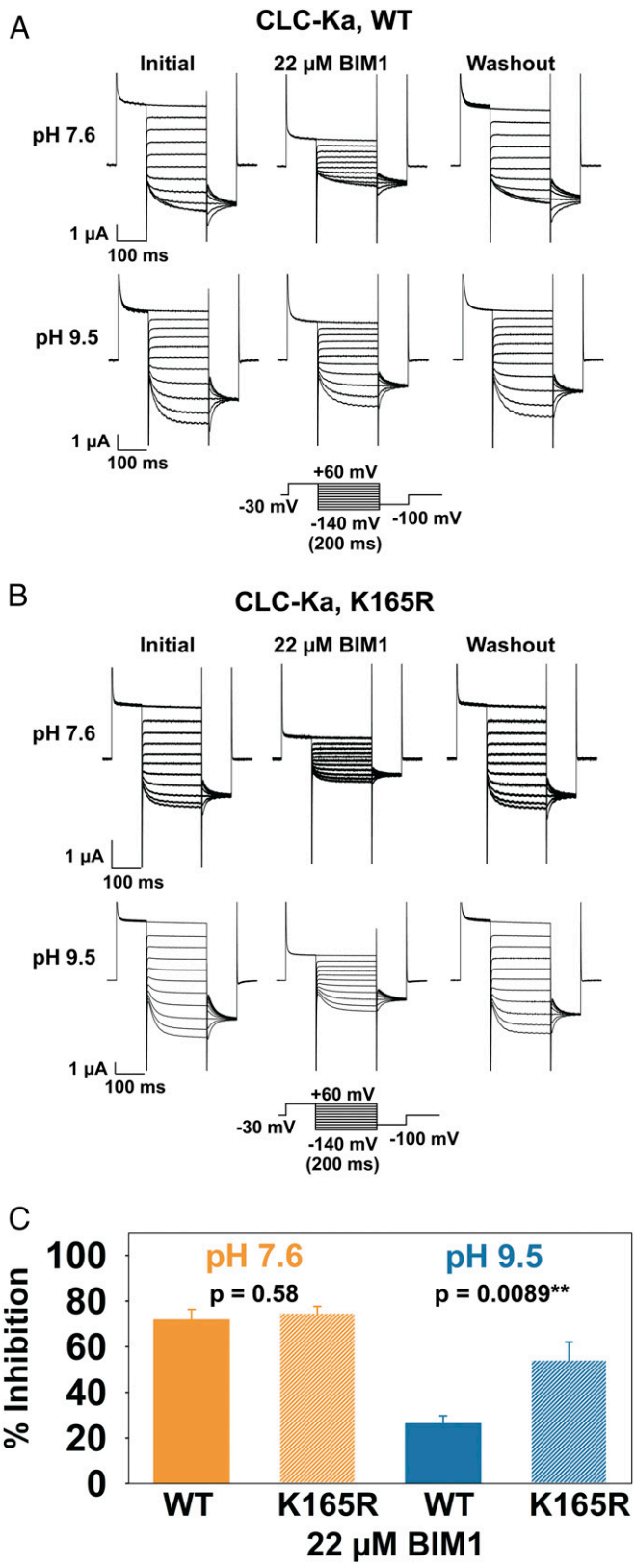

Fig. 6. Testing the docking model: titrating the charge at residue 165. Representative CLC-Ka WT (*A*) or K165R (*B*) currents at pH 7.6 or 9.5, showing responses to 22 μM BIM. (*C*) Summary graph shows the mean ± SEM for the WT, pH 7.6 (71.8 ± 4.6, $n = 4$); K165R, pH 7.6 (74.8 ± 2.9, $n = 5$); the WT, pH 9.5 (26.3 ± 3.4, $n = 5$); and K165R, pH 9.5 (54.2 ± 7.9, $n = 3$). Oocytes were from two batches (each injected with WT and K165R mRNA and each tested at pH 7.6 and pH 9.5). *P* values were calculated using unpaired *t* tests.

-SO_3^- results in a compound with similar selectivity for CLC-Ka over CLC-Kb compared with BIM1. Replacing either $\mathbf{R^2}$ or $\mathbf{R^6}$ -Cl in BIM1 with a sterically larger -Br group (BIM7, BIM11) has little to no effect on selectivity. Similarly, an isomer of BIM1 in which $\mathbf{R^5}$ = Cl and $\mathbf{R^6}$ = H (BIM12) shows little change in homolog selectivity (albeit the potency of this molecule is reduced from BIM1). Strikingly, Ka/Kb selectivity is completely eroded with the -Br analog of BIM12 (BIM13).

Selective inhibition of CLC-Ka is abolished when a -Ph group is introduced in place of -Cl at $\mathbf{R^5}$ or $\mathbf{R^6}$ (BIM4, BIM5, BIM14). A similar outcome has been noted with benzofuran inhibitors: the $\mathbf{R^6}$-phenyl–substituted RT-93 has an IC_{50} of 7.0 ± 0.9 μM against

PHARMACOLOGY

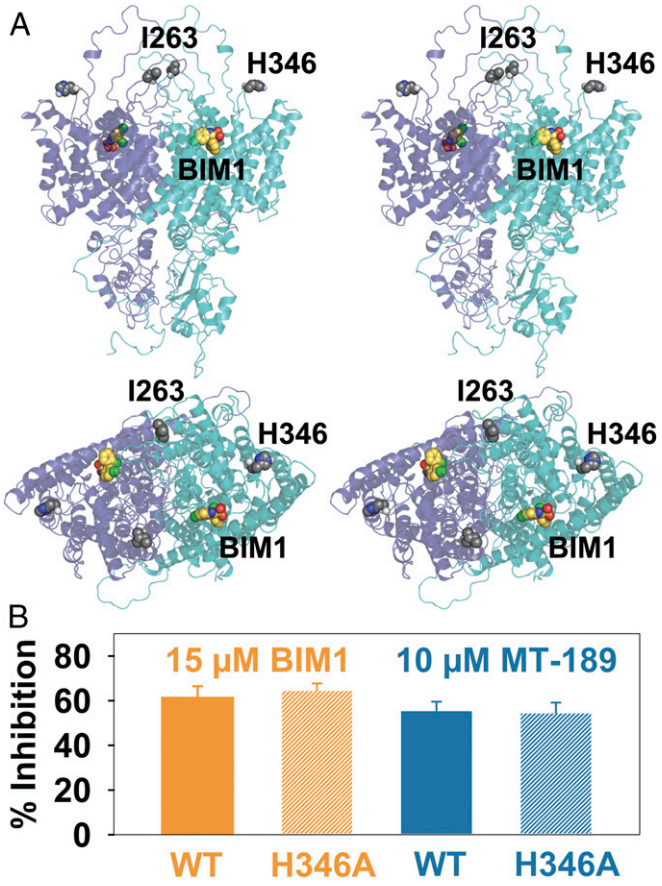

Fig. 7. Testing the prediction of an alternative homology model. (*A*) In our CLC-Ka homology model (Fig. 4), residues I263 and H346 on linkers I–J and K–L are far removed from the inhibitor binding pocket. This is in contrast to an alternative model (30), which places these residues in positions that interact with the bound inhibitor. (*B*) Summary data showing that mutation of H346 has no effect on inhibition by either BIM1 or MT-189. Error bars show the mean ± SEM for measurements on three to five oocytes. Oocytes were from two batches (with one batch used in the experiments comparing BIM1 inhibition of WT and H346A channels and the second batch used in the experiments with MT-189). *P* values (0.53 for BIM1 and 0.66 for MT-189) were calculated using unpaired *t* tests. Representative data traces are shown in Fig. S2.

CLC-Ka and an IC_{50} of 6.0 ± 0.9 μM against CLC-Kb (29). In addition, the recently reported inhibitor SRA-36 (Fig. 1*B*), substituted with a benzyl group at $\mathbf{R^6}$, is equipotent against CLC-Ka and CLC-Kb (30). Loss of Ka/Kb selectivity is also noted for $\mathbf{R^3}$ and $\mathbf{R^4}$ -Ph– and -Br–substituted BIMs (BIM15 to BIM18). Because BIM15 and BIM16 are more potent than BIM1, a comparison of these compounds at a nonsaturating concentration is important to confirm that they are less selective than BIM1. Accordingly, we evaluated inhibition of CLC-Kb by these BIMs at 5 μM (Table S4) and compared selectivity with BIM1 (Fig. S5). These results confirm that BIM15 and BIM16 are substantially less selective between CLC-Ka and CLC-Kb than BIM1.

Our collective findings indicate that the addition of large hydrophobic substituents at positions $\mathbf{R^3}$–$\mathbf{R^6}$ on BIM decreases inhibitor selectivity between the two CLC homologs. The incorporation of -Cl groups at $\mathbf{R^2}$ and $\mathbf{R^6}$, however, is needed to ensure high affinity and selectivity of BIM1 toward CLC-Ka. Other substituents at these two sites that are similar in size and/or polarity to -Cl may further enhance potency and selectivity in next generation inhibitor designs.

Identifying the Heterocycle as Critical for CLC Homolog Selectivity. The structure of BIM1 differs from MT-189 in both the nature of the anionic substituent at $\mathbf{R^1}$ (sulfonate vs. carboxylate) and the structure of the heterocycle (benzimidazole vs. benzofuran). Previous investigations with MT-189 analogs concluded that replacement of the benzofuran heterocycles with either indole or benzothiophene does not alter potency toward CLC-Ka (29) and that a sulfonate group in place of carboxylate anion reduces potency (30). These studies did not query the effect of such structural changes on homolog selectivity.

Based on our studies with DIDS derivatives, we had hypothesized that the sulfonate group in BIM1 would confer increased selectivity for CLC-Ka compared with the analogous carboxylate derivative. To test this hypothesis, we synthesized a set of four compounds and evaluated the potency of these ligands against CLC-Ka and CLC-Kb (Fig. 9). The results clearly show that the enhanced selectivity of BIM1 is dominated by the structure of the heterocycle and not the sulfonate group. Both benzofuran derivatives, MT-189 and AK2-168, exhibit reduced selectivity for CLC-Ka over CLC-Kb compared with analogous benzimidazoles, BIM1 and BIM2. The choice of sulfonate or carboxylate in both the benzofuran and benzimidazole series has little influence on potency and selectivity.

A Rationale for BIM1 Selectivity. What accounts for the enhanced selectivity afforded by the benzimidazole heterocycle in BIM1? We attempted to address this question by comparing the docking results for BIM1 and MT-189. Due to the 10-fold difference in BIM1 and MT-189 potency toward CLC-Kb [IC_{50} = 200 ± 20 μM for BIM1 vs. 20 ± 2 μM for MT-189 (29)], we first examined our CLC-Kb models, looking for specific amino acid side-chain interactions with the heterocyclic scaffolds that could explain the reduced inhibitor potency toward this homolog. (In this analysis, we focused on the bCLC-K–derived homology models.) Analysis of the top nine docking poses for each model suggests that both BIM1 and MT-189 can adopt a variety of orientations in the binding pocket and does not reveal a preference for the benzofuran heterocycle over the benzimidazole heterocycle. Both BIM1 and MT-189 dock to CLC-K models with a biaryl dihedral angle of ∼90° (Fig. S6). These observations are consistent with our initial hypothesis that the BIM scaffold preferentially adopts a noncoplanar conformation (Fig. 1*C*) but do not provide insight into the selectivity difference between BIM1 and MT-189, as none of the predicted ligand–protein interactions seem manifestly responsible for selectivity. Estimating from the measured IC_{50} values, the difference in binding energy that accounts for the selectivity of BIM1 for CLC-Ka over CLC-Kb is likely <2 kcal/mol. By the same logic, the energetic preference of MT-189 for CLC-Kb compared with BIM1 is even smaller. Given the resolution limitations of homology modeling, it is, therefore, not surprising that in silico modeling on this system is insufficient to elucidate the elements responsible for the enhanced selectivity of BIM1.

While our models do not reveal any specific protein–heterocyclic interactions to account for BIM1 selectivity, general differences are evident in the electrostatic surface potentials of the ligand binding pockets in CLC-Ka and CLC-Kb. Models based on either of the two bCLC-K structures indicate that the inhibitor binding site in CLC-Kb is qualitatively more hydrophobic than that of CLC-Ka (Fig. 10). To examine whether there is a link between inhibitor hydrophobicity and CLC-Ka/CLC-Kb selectivity, we calculated logP (cLogP) values for the four analogous benzimidazole and benzofuran derivatives (Fig. 9) using three different cLogP calculators. To isolate the effect of the heterocycle on overall hydrophobicity, we compared compounds with equivalent anionic groups: BIM1 with AK2-168 and BIM2 with MT-189. Across all calculation methods, the trend that emerges is that benzofuran cLogP values are generally higher than those of the corresponding benzimidazoles (Table 1). This trend is consistent with the experimental LogP values reported for the unfunctionalized benzimidazole and benzofuran heterocycles (1.32 for benzimidazole and 2.67 for benzofuran) (Table 1) (40), which indicate that benzofuran is inherently more hydrophobic than benzimidazole. Addition of nonpolar substituents, such as -Br and -Ph, often negates any gains in selectivity achieved by the

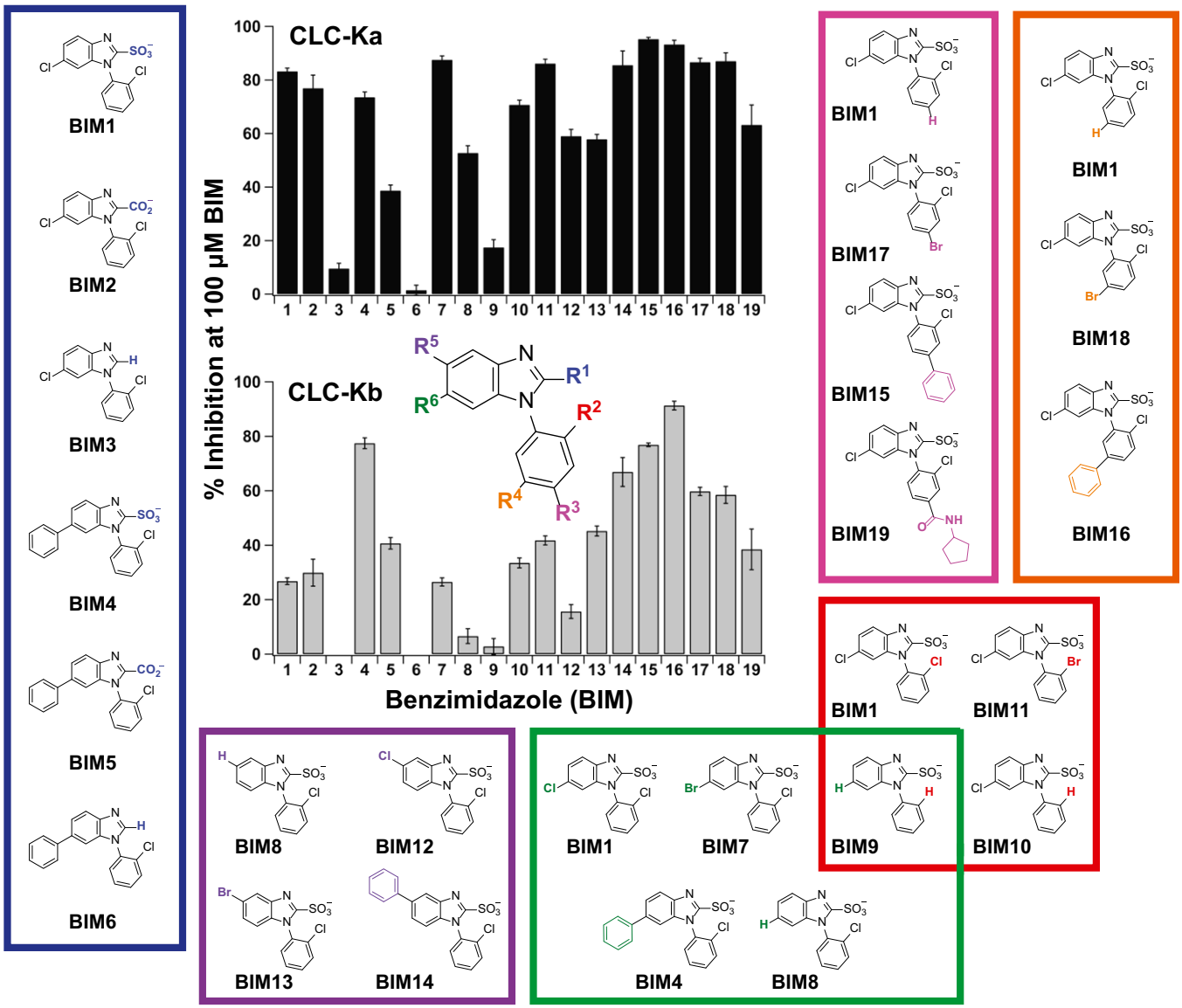

Fig. 8. SARs of BIM inhibitors; 19 BIM variants were synthesized and evaluated. Inhibitor structures are shown, such that each boxed group contains variations at one of the ring positions: R^1 (blue), R^2 (red), R^3 (pink), R^4 (orange), R^5 (magenta), or R^6 (green). The ring positions are correspondingly labeled and colored on the diagram of the BIM scaffold shown in *Middle Center*. Bar graphs show summary inhibition data (mean ± SEM for measurements on 3–17 oocytes) (Table S3).

BIM heterocycle (Fig. 8 and Fig. S5). These observations support our hypothesis that the more polar BIM scaffold (BIM1) disfavors the more hydrophobic CLC-Kb binding site compared with the analogous benzofuran derivative (MT-189) and inhibitors bearing large hydrophobic substituents (BIM4 and BIM5 as well as BIM14 to BIM16). Such insights will aid efforts to further develop CLC-Ka inhibitors with increased potency and homolog selectivity.

Conclusions

The CLC family represents an important class of membrane proteins for which our understanding of physiological function is incomplete and the therapeutic potential is unexplored. We have developed a class of benzimidazole inhibitors that shows unprecedented selectivity toward a single CLC homolog, CLC-Ka, which shares >90% sequence identity with its nearest relative. The modularity of our ligand design and the short synthetic route that we developed provide ready access to a range of inhibitor structures. Through computational modeling and experimental mutagenesis studies, we identified and validated the inhibitor binding site. We also provided evidence that the polarity of the heterocyclic scaffold is driving inhibitor selectivity for CLC-Ka over CLC-Kb. Next generation CLC-Ka inhibitors will explore additional variations of the BIM core, maintaining the optimum twisted biaryl geometry of BIM1 while minimizing the addition of hydrophobic substituents. Inhibitor design will be guided by our CLC-K models based on high-resolution CLC-K structures in combination with protein mutagenesis experiments. This work serves as a foundation for developing and optimizing potent small molecule modulators of specific CLC homologs.

Materials and Methods

Chemical Synthesis. All reagents were obtained commercially unless otherwise noted. Organic solutions were concentrated under reduced pressure (~20 torr) by rotary evaporation. Air- and moisture-sensitive liquids and solutions were transferred via syringe or stainless steel cannula. Chromatographic purification of sulfonate products was accomplished using HPLC on a C18 column (Alltima C18, 10 μM, 22 × 250 mm or SiliaChrom AQ C18, 5 μM,

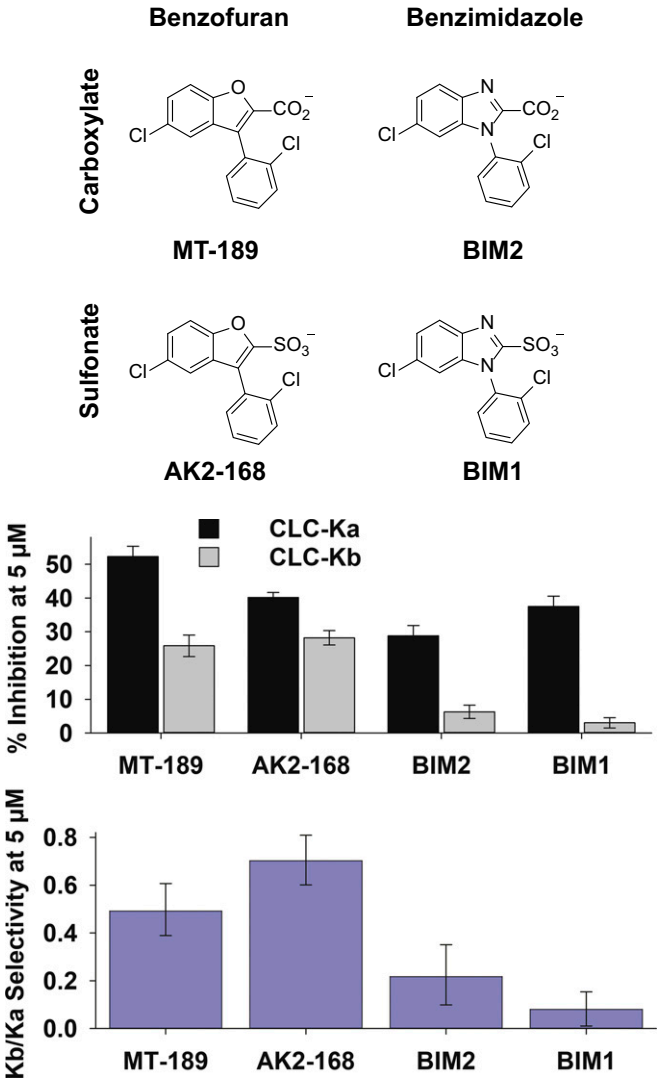

Fig. 9. Investigating the role of the heterocycle and anion substituent on CLC-Ka/CLC-Kb selectivity. Inhibitors synthesized to systematically vary the heterocycle (benzofuran vs. benzimidazole) and the anionic substituent (carboxylate vs. sulfonate) are shown in *Top*. Data for inhibition of CLC-Ka and CLC-Kb by 5 μM of each compound are summarized below (mean ± SEM for measurements on 4–16 oocytes) (Table S4). Each set of experiments was performed on oocytes from two or more separate batches. *Bottom* (purple bars) shows selectivity as reflected by the ratio of percent inhibition of CLC-Kb and CLC-Ka by 5 μM BIM compound. Error bars show 90% CIs computed by the method of Fieller (55) using GraphPad software. The selectivity ratio is shown as CLC-Kb/CLC-Ka, because the inverse ratio would not allow accurate estimation of CIs (56).

10 × 250 mm). TLC was performed on EM Science silica gel 60 F254 plates (250 mm). Visualization of the developed chromatogram was accomplished by fluorescence quenching and by staining with aqueous potassium permanganate or aqueous ceric ammonium molybdate solution.

NMR spectra were acquired on a Varian Inova spectrometer operating at 400, 500, or 600 MHz for ^{1}H and are referenced internally according to residual solvent signals. Data for ^{1}H NMR are recorded as follows: chemical shift (δ; parts per million), multiplicity (singlet, doublet, triplet, quartet, quintet, multiplet, broad), coupling constant (hertz), and integration. Compound concentrations were determined by quantitative NMR in DMSO-d_6 using *N*,*N*-dimethylformamide as an internal standard. IR spectra were recorded as thin films using NaCl plates on a Thermo-Nicolet 300 FT-IR spectrometer and are reported in frequency of absorption. Low-resolution and high-resolution mass spectra were obtained from the Vincent Coates Foundation Mass Spectrometry Laboratory at Stanford University. Detailed synthesis protocols and characterization data for all inhibitors are provided in Dataset S1.

CLC Expression in *Xenopus* Oocytes. Human CLC-Ka, CLC-Kb, CLC-1, and Barttin constructs subcloned into the psGEM vector (41) were linearized with NheI (New England Biolabs) and cleaned using the DNA Clean & Concentrator-5 Kit (Zymo Research) or the Monarch PCR and DNA Reaction Cleanup Kit (New England Biolabs). The linearized plasmids were then transcribed in vitro using the mMESSAGE mMACHINE T7 Kit (Ambion; Life Technologies) and cleaned using the RNeasy MinElute Cleanup Kit (Qiagen) or a classical chloroform:phenol extraction (42). The Y98A mutation was introduced into the Barttin construct, because this mutation increases surface expression of CLC-K channels (22). All mutations were generated using the QuikChange Lightning Site-Directed Mutagenesis Kit (Agilent Technologies). The entire gene was sequenced to confirm occurrence of a desired mutation as well as the absence of additional mutations.

Rat CLC-2 subcloned into the pTLN plasmid vector (43) was linearized with MluI (New England Biolabs). The linearized plasmid was then transcribed in vitro using the mMESSAGE mMACHINE SP6 Kit (Ambion; Life Technologies)

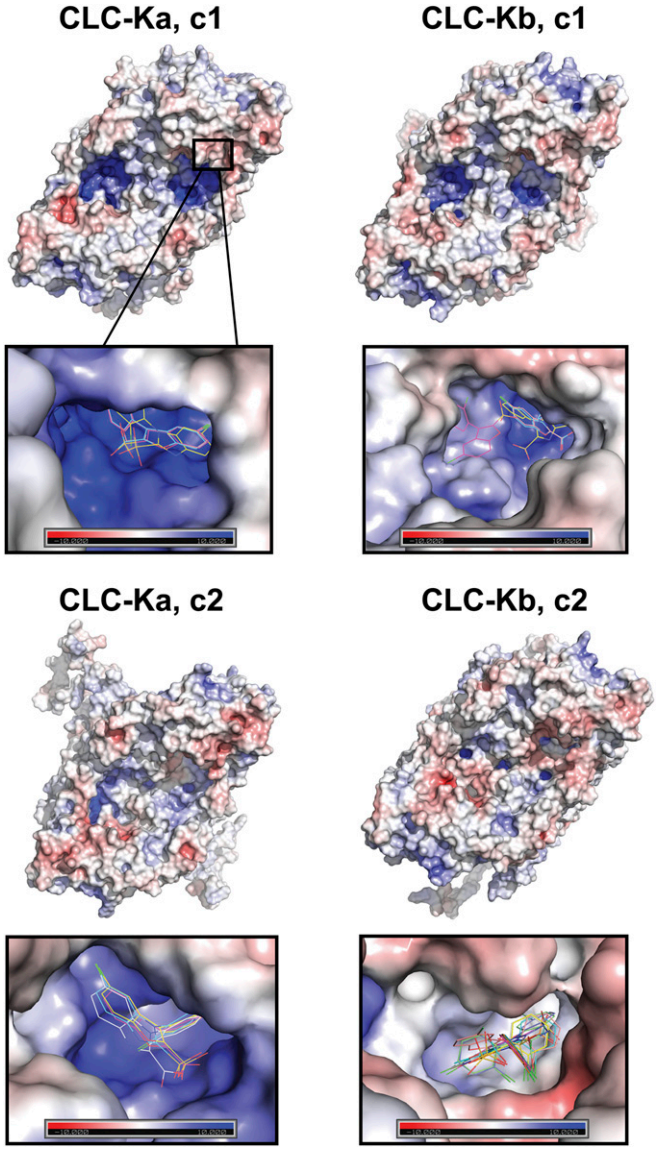

Fig. 10. A rationale for BIM selectivity—evaluating hydrophobicity of inhibitor binding sites. Electrostatic surface maps of the CLC-Ka and CLC-Kb homology models viewed from the extracellular side; scale is from −10 kT/e (red; negative) to +10 kT/e (blue; positive). These models, based on the two cryo-EM structures of bCLC-K (c1 and c2), reveal the CLC-Kb inhibitor binding pocket to be more hydrophobic than that of CLC-Ka. Molecules shown in the binding sites are a collection of representative docking poses for BIM1, BIM2, MT-189, and AK2-168 within each of four models.

Table 1. Evaluating inhibitor hydrophobicity

Compound	Experimental LogP	cLogP QikProp	cLogP MolInspiration	cLogP ChemDraw
BIM1	—	2.89	1.74	2.34
AK2-168	—	3.27	2.55	2.98
BIM2	—	3.56	3.94	5.42
MT-189	—	4.07	5.08	4.79
Benzimidazole	1.32	1.32	1.43	1.57
Benzofuran	2.67	2.61	2.26	2.70

Hydrophobicity of benzimidazoles vs. benzofurans. Three different computational algorithms were used to determine the cLogP values [for the set of inhibitors examined in Fig. 9 and for unsubstituted benzimidazole and benzofuran, for which experimental values are available (Table S5)].

and purified as described for the other constructs. For some CLC-2 experiments, an alternate construct was used in an attempt to boost expression levels. Rat CLC-2 was codon optimized for *Xenopus* and subcloned into the pUNIV plasmid with the addition of a 3′ β-globin UTR at the end of the gene (44). The pUNIV construct was linearized with NotI (New England Biolabs) and transcribed in vitro using the mMESSAGE mMACHINE T7 Kit (Ambion; Life Technologies). Expression levels were found to be similar for both constructs.

Electrophysiology. Defolliculated *Xenopus* oocytes were injected with 27.6–50.6 nL of cRNA at 0.2–1.5 μg/μL: 5–40 ng for CLC-K:Y98A-Barttin (2:1 mixture), 4–8 ng for CLC-1, and 19–37 ng for CLC-2. Oocyte storage and recording solutions are described in *SI Materials and Methods*. All data were collected using an Oocyte Clamp OC-725C amplifier (Warner Instruments) interfaced with Digidata 1322A and pClamp 9.2 software (Axon Instruments) at room temperature (~20 °C). The data were sampled at 10 kHz and low pass-filtered at 1 kHz. Currents were measured using voltage protocols as indicated in the figures. For CLC-Kb, the test pulse duration (500 ms) was longer than that used for CLC-Ka (200 ms) because of the slower kinetics of CLC-Kb and hence, the longer time required to reach steady state at negative voltages. The membrane potential was held at the resting potential (usually −30 mV) during the intersweep interval between each voltage step, with a total time of 1–2 s per sweep.

Solution changes were done by perfusing the chamber with 4–5 mL of each solution (~15 times the volume of the chamber) at ~1 mL/min using Baxter Control-A-Flo regulators or manual pipetting. The fraction of current remaining after steady-state inhibition (percentage inhibition) was calculated using the currents measured in the presence and absence of inhibitors. For most experiments, background current from endogenous *Xenopus* anion currents was subtracted using an iodide block protocol that is based on the observation that iodide inhibits CLC-K currents but not endogenous *Xenopus* anion currents (35). At the end of each experiment on CLC-K channels, oocytes were exchanged into a solution containing 100 mM NaI (with 5 mM $MgSO_4$, 5 mM Na-Hepes, pH 7.6, adjusted with NaOH). The contribution of endogenous currents was evaluated based on current remaining in the presence of 100 mM iodide at +60 mV. Endogenous currents at lower voltages (down to −140 mV) were estimated by linear extrapolation of the endogenous currents at +60 mV (35). Endogenous currents were subtracted from recorded currents with and without inhibitor present. This background correction was performed for all CLC-K experiments with two exceptions. (*i*) For the 19-compound screen at 100 μM (Fig. 8), the absence of background correction in this set of experiments results in a slight underestimation of percentage inhibition but still allows for across the board comparison of relative efficacy of each BIM derivative examined. (*ii*) For experiments using 300 μM BIM1 (Figs. 2 and 5), the NaI subtraction protocol became inaccurate, since BIM1 at this high concentration was found to inhibit endogenous currents. To correct for background currents in experiments with 300 μM BIM1, currents from three to five uninjected oocytes from the same batch were averaged and used for subtraction of background current and subsequent calculation of percentage inhibition as described below. For CLC-1 and CLC-2 experiments, the NaI subtraction protocol cannot be performed, since these homologs are not completely blocked by iodide (43, 45). Given that BIM1 does not significantly inhibit either CLC-1 or CLC-2 (Fig. 3), subtraction of background currents was not necessary.

To calculate percentage inhibition of CLC-K current, currents measured in response to the voltage steps (steps that follow the prepulse to +60 mV) (protocols are depicted in Fig. 2) were analyzed. An average of 15 ms of data, taken from within the last 25 ms of each of the current traces, was determined for currents measured before addition of inhibitor ("initial"), after addition of inhibitor ("inhibited"), after washout of inhibitor ("washout"), and after switching to 100 mM NaI ("NaI"). To obtain background-corrected currents, the NaI currents (or currents from uninjected oocytes as described above) were subtracted from each of the initial, inhibited, and washout currents. Percentage inhibition was determined using these background-corrected currents. Data reported in the figures reflect inhibition determined by dividing the background-corrected inhibited current by the initial current (and multiplying by 100). Experiments in which there was poor reversibility of inhibition were discarded; poor reversibility was defined as cases in which reversal current differed by >20% from initial current and/or inhibition calculated using washout current differed by >10% from inhibition calculated using initial current. Percentage inhibition was plotted as a function of inhibitor concentration and fitted to a sigmoid function using Sigmaplot 13.0 (Systat Software) to obtain IC_{50} values. Summary data report inhibition at +60 mV unless otherwise noted (Fig. 3 and Fig. S1). To calculate percentage inhibition of CLC-1 or CLC-2 current, an average of 5 ms (CLC-1) or 17 ms (CLC-2) of the current trace within the final portion of each test pulse was determined.

Homology Model Generation. First generation human CLC-Ka and CLC-Kb models were created from the structural PDB templates of the eukaryotic CLC transporter cmCLC (PDB ID code 3org) and the water-soluble cytoplasmic domain of human CLC-Ka (PDB ID code 2pfi). Target template amino acid sequence alignments were created using the FFAS03 protocol for profile–profile alignments (46) and used for the initial modeling procedure. The template sequences were ~30% identical (40% similar) to the target CLC-Ka and CLC-Kb sequences. C-α atoms in the two subunits were symmetrically constrained during model generation given the C2 symmetry of dimeric CLC protein structures. One Ca^{2+} ion was added to cytoplasmic loop residues (47) E259, E261, D278, and E281 in each subunit using spatial restraints.

One thousand preliminary models were built using MODELER 9.12 (48). The five models with the lowest MODELER objective function were kept for further evaluation by the homology model-scoring program ProQ (49) and the crystallographic model assessment tools Procheck (50) and What-If (51). The overall best-scoring model was selected as the final model for docking simulations.

Second generation human CLC-Ka and CLC-Kb models were created from structural templates of bCLC-K. The structure of this template protein, determined using single-particle cryo-EM, revealed two different conformations denoted c1 and c2 (PDB ID codes 5tqq and 5tr1, respectively) (39). The major difference between the two conformations is an ~6° rigid body rotation of the transmembrane regions within each subunit that results in a change at the subunit interface; the Cl^- permeation pathways within each of the two conformations are similar to one another (39). Both the c1 and c2 conformations were used to model CLC-Ka and CLC-Kb, rendering a total of four protein models based on bCLC-K. Because the overall target template sequence identity is ~84%, these template structures likely represent a better structural framework for modeling than PDB ID code 3org.

Electrostatic surface maps were generated using the Adaptive Poisson-Boltzmann Solver plugin for PyMol and are depicted as surface potentials in Fig. 10.

Molecular Docking. Inhibitor molecules were drawn using MarvinSketch 14.10.13 and converted to .pdbqt format using AutoDock. Initial docking trials of our first generation CLC-K models were performed using with AutoDock 4.2 (52) using a grid spacing of 0.375 Å. A search box surrounding the extracellular surface of the protein model was defined, in which 1,000 searches were carried out using the Lamarckian Genetic Algorithm. For each search, 2.5×10^6 energy evaluations were calculated. After structural rms clustering, lowest docked energy conformations of inhibitors were found docked at the N68/D68-K165 site. Final docking trials were performed using AutoDock Vina (53). Searches were centered at the N68/D68-K165 site using a search box of 22 × 22 × 22 Å in *x*, *y*, and *z* dimensions. Two docking protocols were carried out: one treating the model residues as rigid ("rigid docking protocol") and another where residues in the vicinity of the inhibitor binding pocket were allowed flexibility during the docking search algorithm ("flexible docking protocol"). In the flexible docking protocol, residues N/D68, K165, F250, L253, and K355 were allowed flexibility. Both docking protocols yielded similar results.

Molecular docking to our second generation models based on bCLC-K was carried out using Autodock Vina. Preliminary docking trials identified the region near N68 and F250 in both the c1 and c2 models discussed above. Rigid and flexible docking protocols were carried out using a search box of 28 × 28 × 28 Å that encompasses this region in our protein models for CLC-Ka and CLC-Kb. Two flexible docking protocols were performed. As a direct comparison with our original homology model, the same five residues were allowed flexibility: N/D68, K165, F250, L253, and K355. In the second flexible

docking protocol, 13 (CLC-Ka) or 14 (CLC-Kb) residues were allowed flexibility: N/D68, I/V71, E72 (CLC-Kb), V75, L155, L163, K165, S258, Q260, S353, M354, K355, L358 , M427. These residues were chosen based on the results of our rigid docking protocol to our bCLC-K models together with our experimental site-directed mutagenesis data. The top-scoring BIM1 docking pose for the c1 CLC-Ka model predicts BIM1 interactions with N68 and K165 as validated through site-directed mutagenesis, and the remaining residues are those within 8 Å of the bound molecule for the top-scoring pose. The second flexible docking protocol was performed only on the c1 CLC-Ka and CLC-Kb models. The top nine poses (with the lowest docking energies) from each set of docking protocols were compared as described in the text and Fig. S6.

Partition Coefficient Analysis. Octanol/water partition coefficients (cLogP) were calculated by three different methods for the protonated form of each molecule (Table 1): ChemDraw software suite (version 14.0), MolInspiration (www.molinspiration.com; 2017), and Schrödinger QikProp (version 2017–3). For Schrödinger QikProp, molecular structures were first optimized using the OPLS3 force field (54). Experimental LogP values for related heterocycles (Table S5) are the preferred values compiled by Hansch et al. (40) for the neutral form of each molecule unless otherwise noted. For comparison and validation of the cLogP calculation methods, values were calculated for molecules with known experimental LogP values in the test set reported in Table S5.

ACKNOWLEDGMENTS. We thank Chien-Ling Lee for performing the experiments to test sensitivity of CLC-1 and CLC-2 to BIM1. We also thank Dr. Thomas Jentsch for providing CLC-Ka, CLC-Kb, Barttin, CLC-1, and CLC-2 DNA. This research was supported by American Heart Association (AHA) Grants 10GRNT3890045 (to M.M.) and 1GRNT16940072 (to M.M.) and a Stanford Bio-X Seed Grant (to M.M. and J.D.B.). A.K.K. was supported by the Stanford Center for Molecular Analysis and Design (CMAD) and a Stanford Interdisciplinary Graduate Fellowship (SIGF) through the Stanford Chemistry, Engineering, & Medicine for Human Health (ChEM-H) Institute. C.A.P.W. was supported by an HHMI undergraduate fellowship and a Stanford Graduate Fellowship in Science and Engineering. R.T.-T. is the recipient of a Graduate Research Fellowship from the National Science Foundation. T.S.C. was supported by a Stanford School of Medicine Dean's Postdoctoral Fellowship and AHA Grant 17POST33670553. J.A. thanks Verket För Innovationssystem for financial support.

1. Jentsch TJ (2015) Discovery of CLC transport proteins: Cloning, structure, function and pathophysiology. *J Physiol* 593:4091–4109.
2. Stölting G, Fischer M, Fahlke C (2014) CLC channel function and dysfunction in health and disease. *Front Physiol* 5:378.
3. Stauber T, Weinert S, Jentsch TJ (2012) Cell biology and physiology of CLC chloride channels and transporters. *Compr Physiol* 2:1701–1744.
4. Jentsch TJ (2008) CLC chloride channels and transporters: From genes to protein structure, pathology and physiology. *Crit Rev Biochem Mol Biol* 43:3–36.
5. Abeyrathne PD, Chami M, Stahlberg H (2016) Biochemical and biophysical approaches to study the structure and function of the chloride channel (ClC) family of proteins. *Biochimie* 128-129:154–162.
6. Miller C (2015) In the beginning: A personal reminiscence on the origin and legacy of ClC-0, the 'Torpedo Cl(-) channel'. *J Physiol* 593:4085–4090.
7. Accardi A (2015) Structure and gating of CLC channels and exchangers. *J Physiol* 593: 4129–4138.
8. Zifarelli G, Pusch M (2007) CLC chloride channels and transporters: A biophysical and physiological perspective. *Reviews of Physiology, Biochemistry and Pharmacology*, ed Amara SG (Springer, Berlin), pp 23–76.
9. Miller C (2006) ClC chloride channels viewed through a transporter lens. *Nature* 440: 484–489.
10. Maduke M, Miller C, Mindell JA (2000) A decade of CLC chloride channels: Structure, mechanism, and many unsettled questions. *Annu Rev Biophys Biomol Struct* 29:411–438.
11. Poroca DR, Pelis RM, Chappe VM (2017) ClC channels and transporters: Structure, physiological functions, and implications in human chloride channelopathies. *Front Pharmacol* 8:151.
12. Zaika O, Tomilin V, Mamenko M, Bhalla V, Pochynyuk O (2016) New perspective of ClC-Kb/2 Cl- channel physiology in the distal renal tubule. *Am J Physiol Renal Physiol* 310:F923–F930.
13. Imbrici P, et al. (2015) ClC-1 chloride channels: State-of-the-art research and future challenges. *Front Cell Neurosci* 9:156.
14. Verkman AS, Galietta LJV (2009) Chloride channels as drug targets. *Nat Rev Drug Discov* 8:153–171.
15. Suh KS, Yuspa SH (2005) Intracellular chloride channels: Critical mediators of cell viability and potential targets for cancer therapy. *Curr Pharm Des* 11:2753–2764.
16. Simon DB, et al. (1997) Mutations in the chloride channel gene, CLCNKB, cause Bartter's syndrome type III. *Nat Genet* 17:171–178.
17. Uchida S (2000) Physiological role of CLC-K1 chloride channel in the kidney. *Nephrol Dial Transplant* 15(Suppl 6):14–15.
18. Matsumura Y, et al. (1999) Overt nephrogenic diabetes insipidus in mice lacking the CLC-K1 chloride channel. *Nat Genet* 21:95–98.
19. Denton JS, Pao AC, Maduke M (2013) Novel diuretic targets. *Am J Physiol Renal Physiol* 305:F931–F942.
20. Buffington MA, Abreo K (2016) Hyponatremia: A review. *J Intensive Care Med* 31: 223–236.
21. McGreal K, Budhiraja P, Jain N, Yu ASL (2016) Current challenges in the evaluation and management of hyponatremia. *Kidney Dis (Basel)* 2:56–63.
22. Estévez R, et al. (2001) Barttin is a Cl- channel β-subunit crucial for renal Cl- reabsorption and inner ear K+ secretion. *Nature* 414:558–561.
23. Thompson CH, et al. (2009) Isolation and characterization of a high affinity peptide inhibitor of ClC-2 chloride channels. *J Biol Chem* 284:26051–26062.
24. Salhany JM (1996) Allosteric effects in stilbenedisulfonate binding to band 3 protein (AE1). *Cell Mol Biol* 42:1065–1096.
25. Romero MF, Chen A-P, Parker MD, Boron WF (2013) The SLC4 family of bicarbonate (HCO_3^-) transporters. *Mol Aspects Med* 34:159–182.
26. Cabantchik ZI, Greger R (1992) Chemical probes for anion transporters of mammalian cell membranes. *Am J Physiol* 262:C803–C827.
27. Miller C, White MM (1984) Dimeric structure of single chloride channels from Torpedo electroplax. *Proc Natl Acad Sci USA* 81:2772–2775.
28. Matulef K, et al. (2008) Discovery of potent CLC chloride channel inhibitors. *ACS Chem Biol* 3:419–428.
29. Liantonio A, et al. (2008) Molecular switch for CLC-K Cl- channel block/activation: Optimal pharmacophoric requirements towards high-affinity ligands. *Proc Natl Acad Sci USA* 105:1369–1373.
30. Liantonio A, et al. (2016) Kidney CLC-K chloride channels inhibitors: Structure-based studies and efficacy in hypertension and associated CLC-K polymorphisms. *J Hypertens* 34:981–992.
31. Hartzell HC (2010) Chloride channels: An historical perspective. *Physiology and Pathology of Chloride Transporters and Channels in the Nervous System: From Molecules to Diseases*, eds Alvarez-Leefmans F, Delpire E (Academic, San Diego), 1st Ed, pp 3–15.
32. Feng L, Campbell EB, Hsiung Y, MacKinnon R (2010) Structure of a eukaryotic CLC transporter defines an intermediate state in the transport cycle. *Science* 330:635–641.
33. Markovic S, Dutzler R (2007) The structure of the cytoplasmic domain of the chloride channel ClC-Ka reveals a conserved interaction interface. *Structure* 15:715–725.
34. Gradogna A, Pusch M (2010) Molecular pharmacology of kidney and inner ear CLC-K chloride channels. *Front Pharmacol* 1:130.
35. Picollo A, et al. (2004) Molecular determinants of differential pore blocking of kidney CLC-K chloride channels. *EMBO Rep* 5:584–589.
36. Liantonio A, et al. (2006) Activation and inhibition of kidney CLC-K chloride channels by fenamates. *Mol Pharmacol* 69:165–173.
37. Gradogna A, Pusch M (2013) Alkaline pH block of CLC-K kidney chloride channels mediated by a pore lysine residue. *Biophys J* 105:80–90.
38. Pace CN, Grimsley GR, Scholtz JM (2009) Protein ionizable groups: pK values and their contribution to protein stability and solubility. *J Biol Chem* 284:13285–13289.
39. Park E, Campbell EB, MacKinnon R (2017) Structure of a CLC chloride ion channel by cryo-electron microscopy. *Nature* 541:500–505.
40. Hansch C, Leo A, Hoekman D (1995) *Exploring QSAR: Hydrophobic, Electronic, and Steric Constants* (Am Chem Soc, Washington, DC).
41. Martinez GQ, Maduke M (2008) A cytoplasmic domain mutation in ClC-Kb affects long-distance communication across the membrane. *PLoS One* 3:e2746.
42. Sambrook J, Russell DW (2006) Purification of nucleic acids by extraction with phenol: chloroform. *CSH Protoc* 2006:pdb.prot4455.
43. Lorenz C, Pusch M, Jentsch TJ (1996) Heteromultimeric CLC chloride channels with novel properties. *Proc Natl Acad Sci USA* 93:13362–13366.
44. Venkatachalan SP, et al. (2007) Optimized expression vector for ion channel studies in Xenopus oocytes and mammalian cells using alfalfa mosaic virus. *Pflugers Arch* 454:155–163.
45. Rychkov GY, Pusch M, Roberts ML, Jentsch TJ, Bretag AH (1998) Permeation and block of the skeletal muscle chloride channel, ClC-1, by foreign anions. *J Gen Physiol* 111:653–665.
46. Jaroszewski L, Rychlewski L, Godzik A (2000) Improving the quality of twilight-zone alignments. *Protein Sci* 9:1487–1496.
47. Gradogna A, Fenollar-Ferrer C, Forrest LR, Pusch M (2012) Dissecting a regulatory calcium-binding site of CLC-K kidney chloride channels. *J Gen Physiol* 140:681–696.
48. Šali A, Blundell TL (1993) Comparative protein modelling by satisfaction of spatial restraints. *J Mol Biol* 234:779–815.
49. Wallner B, Elofsson A (2003) Can correct protein models be identified? *Protein Sci* 12: 1073–1086.
50. Morris AL, MacArthur MW, Hutchinson EG, Thornton JM (1992) Stereochemical quality of protein structure coordinates. *Proteins* 12:345–364.
51. Hooft RWW, Vriend G, Sander C, Abola EE (1996) Errors in protein structures. *Nature* 381:272.
52. Morris GM, et al. (2009) AutoDock4 and AutoDockTools4: Automated docking with selective receptor flexibility. *J Comput Chem* 30:2785–2791.
53. Trott O, Olson AJ (2010) AutoDock Vina: Improving the speed and accuracy of docking with a new scoring function, efficient optimization, and multithreading. *J Comput Chem* 31:455–461.
54. Harder E, et al. (2016) OPLS3: A force field providing broad coverage of drug-like small molecules and proteins. *J Chem Theory Comput* 12:281–296.
55. Fieller EC (1940) The biological standardization of insulin. *Suppl J R Stat Soc* 7:1–64.
56. Motulsky H (2007) *Intuitive Biostatistics* (Oxford Univ Press, New York).